INTERNATIONAL JOURNAL FOR NUMERICAL AND ANALYTICAL METHODS IN GEOMECHANICS
Int. J. Numer. Anal. Meth. Geomech., **22**, 449–475 (1998)

COUPLED CONSOLIDATION OF A POROUS MEDIUM WITH A CYLINDRICAL OR A SPHERICAL CAVITY

Y. ZHOU, R. K. N. D. RAJAPAKSE* AND J. GRAHAM

Department of Civil and Geological Engineering, University of Manitoba, 15, Gillson St., Winnipeg, Canada R3T 5V6

SUMMARY

This paper presents a theoretical approach to analyse coupled, linear thermoporoelastic fields in a saturated porous medium under radial and spherical symmetry. The governing equations account for compressibility and thermal expansion of constituents, heat sink due to thermal dilatation of water and thermal expansion of the medium, and *thermodynamically coupled heat–water flow*. It has been reported in the literature that thermodynamically coupled heat–water flows known as *thermo-osmosis* and *thermal filtration* have the potential to significantly alter the flow fields in clay-rich barriers in the near field of a underground waste containment scheme. This study presents a mathematical model and examines the effects of thermo-osmosis and thermal-filtration on coupled consolidation fields in a porous medium with a cavity. Analytical solutions of the governing equations are presented in the Laplace transform space. A numerical inversion scheme is used to obtain the time-domain solutions for a cylindrical cavity in a homogeneous or a non-homogeneous medium. A closed form time-domain solution is presented for a spherical cavity in a homogeneous medium. Selected numerical solutions for homogeneous and non-homogeneous media show a significant increase in pore pressure and displacements due to the presence of thermodynamically coupled flows and a negligible influence on temperature. © 1998 John Wiley & Sons, Ltd.

Key words: consolidation; heat transfer; poroelasticity; pore pressure; coupled fields; Laplace transform

INTRODUCTION

The study of coupled processes in saturated porous materials under gradients of pore water pressure, temperature and deformations is important to several branches of engineering. In recent years, considerable attention has been generated on this topic due to its relevance to the assessment of performance of engineered barriers proposed for underground disposal of radioactive wastes.[1–4] For example, the current Canadian programme for management of nculear fuel waste proposes to store metal canisters containing spent fuel rods in a deep geologic vault built in the Canadian Shield. A sand–bentonite mixture is placed between the canister and the surrounding rock as an integral component of the multi-barrier concept. Heat generated by the waste and the *in situ* pore water pressure gradient could have a significant effect on the performance of an engineered barrier. Excessive drying and shrinkage of a barrier in the vicinity of a waste canister and the possible hydraulic fracture of a barrier due to pore water pressure build-up may result in

*Correspondence to: R. K. N. D. Rajapakse, Department of Civil and Geological Engineering, University of Manitoba, 15, Gillson, St., Winnipeg, Canada R3T 5V6

CCC 0363–9601/98/060449–27$17.50

Received 24 March 1997
Revised 1 October 1997

the breakdown of the multi-barrier concept which is the cornerstone of radioactive waste disposal schemes. Therefore, there is a need to study the response of engineered barriers under various combinations of thermal and hydraulic loading, and boundary conditions.

Past studies[5–15] on coupled thermoporoelastic analysis are based on the assumption that the medium is completely saturated. Engineered barriers may be initially unsaturated and solutions based on fully saturated conditions can only be used as an approximation for such barriers. Another important assumption of past studies is the absence of coupled heat–water flow due to non-conjugate thermodynamic forces. Such coupled flows are a consequence of thermodynamics of irreversible processes when compared to various degrees of 'mathematical coupling' built into Biot[16] types models[5–15] accounting primarily for flow due to conjugate driving forces. Special characteristics of clay-rich barriers of extreme low permeability (10^{-12}–10^{-14} m/s) and large initial near-field temperature gradients ($>20^{\circ}$C/m) in typical waste repositories require the consideration of influence of thermal gradient on pore water flow[4,17–21] (thermo-osmosis) and pore water pressure gradient on heat flow (thermal filtration). Srivastava and Avasthi[19] and Carnahan[20] showed that water flux due to thermo-osmosis can easily exceed Darcy flux in very low permeability clays. Thus, thermo-osmosis has the potential to accelerate the water loss in a barrier leading to shrinkage and excessive build up of pore water pressure. Recently Zhou *et al.*[22] presented a coupled thermoporoelastic theory accounting for thermo-osmosis and thermal filtration, compressibility and thermal expansion of constituents, large variation of temperature, convective heat flow and non-linear material properties. The governing equations of Zhou *et al.*[22] are non-linear even for linear materials if complete coupling between mechanical deformations, heat flow and water flow is considered. A finite element formulation of the non-linear governing equations was also presented. Solutions for coupled linear and non-linear fields in a one-dimensional soil column demonstrated the significance of the thermodynamic coupling and principal features of consolidation fields.

Models accounting for non-linear material behaviour require extensive experimental data and a substantial computational effort in the analysis. On the other hand, linear models require relatively lesser data and can be solved by using analytical methods. Such analytical solutions are often used to gain quick insight into the physics of a complex coupled system, and the influence of various material properties and boundary conditions without performing extensive numerical studies. Linear analytical solutions are also useful in the validation of computer codes developed for non-linear problems.

This study is based on a linearized version of the coupled theory developed by Zhou *et al.*[22] and presents solutions for thermodynamically coupled consolidation fields in domains with radial or spherical symmetry. Such problems are of interest to waste containment studies. In the ensuing sections the governing equations are summarized and analytical general solutions are presented in the Laplace transform domain. These analytical solutions are used to solve problems involving a cylindrical or a spherical cavity in an infinite porous medium. Due to the complexity of Laplace inversion, time-domain solutions for a cylindrical cavity are obtained by using a numerical scheme. A closed form time-domain solution is derived for a spherical cavity subjected to a constant temperature increase. The analysis of non-homogeneous cylindrical and spherical domains is also discussed. Selected numerical solutions for temperature change, pore water pressure and displacement in homogeneous and non-homogeneous media are presented to demonstrate the principal features of coupled fields and the significance of thermodynamic coupling.

GOVERNING EQUATIONS

The poroelastic theory used in the present study is a linearized version of the non-linear theory developed by Zhou *et al.*[22] which allows analytical treatment of the governing equations. Basic assumptions of the linear theory include complete saturation of the medium, continuity of the water phase, thermal equilibrium between solid particles and water, small changes in temperature, absence of phase change of water, isotropy, linear elastic behaviour, constant thermal and hydraulic properties, small displacements and infinitesimal strains. The present theory accounts for thermal expansion and compressibility of constituents and thermodynamically coupled heat–water flow. The basic equations are summarized in the following.

The constitutive relations for linear thermoporoelastic response of an isotropic medium can be expressed in terms of effective stress σ'_{ij} (positive for tension), strain ε_{ij} and temperature change T as

$$\sigma'_{ij} = 2G\left(\varepsilon_{ij} + \delta_{ij}\frac{v}{1-2v}\varepsilon_{kk}\right) - K'\alpha T\delta_{lj} \tag{1}$$

where $\sigma'_{ij} = \sigma_{ij} + \xi p\delta_{ij}$ and σ_{ij} denotes total stress (positive for tension), δ_{ij} is Kronecker's delta, p is the pore water pressure (negative for suction), $\xi \leqslant 1$) is a coefficient which depends on the compressibility of the constituents ($\xi = 1 - K'/K_s$), K_s is the bulk modulus of soil grains, $K'[=(2G(1+v))/(3(1-2v))]$ is the drained bulk modulus of the soil medium, v is the drained Poission's ratio, α is the coefficient of volumetric expansion of soil medium ($^\circ C^{-1}$) and G is the shear modulus.

The equation of equilibrium can be expressed in terms of displacements u_i, water pressure p and temperature change T as

$$G\nabla^2 u_i + \frac{G}{1-2v}u_{j,ji} - \xi p_{,i} - K'\alpha T_{,i} = 0 \tag{2}$$

In the absence of water pressure and temperature gradients, equation (2) reduces to the classical Navier equations.

Equation (2) yields

$$\frac{1-v}{1-2v}2G\nabla^2\varepsilon_v - \xi\nabla^2 p - K'\alpha\nabla^2 T = 0 \tag{3}$$

Consider a saturated soil element of volume V that consists of a volume V_s of soil grains and a volume V_e of voids. Then

$$\frac{1}{V}\frac{\partial V}{\partial t} = \frac{1}{V}\frac{\partial V_e}{\partial t} + \frac{1}{V}\frac{\partial V_s}{\partial t} = \frac{\partial \varepsilon_v}{\partial t} \tag{4}$$

where ε_v is the volume strain.

The change of volume of soil grains is given by

$$\frac{1}{V}\frac{\partial V_s}{\partial t} = (1-n)\alpha_s\frac{\partial T}{\partial t} - \frac{1-n}{K_s}\frac{\partial p}{\partial t} + \frac{1}{3K_s}\mathbf{m}\frac{\partial \boldsymbol{\sigma}'}{\partial t} \tag{5}$$

and

$$\mathbf{m} = \langle 1\ 1\ 1\ 0\ 0\ 0\rangle \tag{6}$$

where n, α_s, and $\boldsymbol{\sigma}'$ denote the porosity, coefficient of volumetric thermal expansion of solid grains and effective stress vector, respectively.[22]

The three terms on the right-hand side of equation (5) represent the volume change of soil grains due to changes of temperature, water pressure and effective stresses, respectively. The bulk odulus of solid grains (K_s) in equation (5) is different for different materials. Limited data are available in literature for K_s and a standard value is often used. The selection of a proper value for K_s is always a problem. On the other hand, the effect of the last two terms of equation (5) is generally very small due to the large value of K_s encountered in most practical situations.

The change in volume of voids is given by

$$\frac{1}{V}\frac{\partial V_e}{\partial t} = -\nabla q_w + n\alpha_w \frac{\partial T}{\partial t} - \frac{n}{\beta_w}\frac{\partial p}{\partial t} \tag{7}$$

where q_w, α_w, and β_w denote the water flux/unit area (m/s), coefficients of volumetric thermal expansion and bulk modulus of pore water.[22] Generally speaking, α_w is a function of temperature. For linear models involving a relatively small variation of temperature a constant average value for α_w can be assumed. The variation of α_w is accounted for in the non-linear model proposed by Zhou *et al.*[22]

Substitution of equations (5) and (7) into equation (4) results in

$$\nabla q_w = -\frac{\partial \varepsilon_v}{\partial t} + [n\alpha_w + (1-n)\alpha_s]\frac{\partial T}{\partial t} - \left(\frac{n}{\beta_w} + \frac{1-n}{K_s}\right)\frac{\partial p}{\partial t} + \frac{1}{3K_s}\mathbf{m}\frac{\partial \boldsymbol{\sigma}'}{\partial t} \tag{8}$$

The second term on the right-hand side of equation (8) can be dropped if thermal expansion of constituents are neglected and the third and fourth terms vanish for a medium with incompressible constituents.

Based on thermodynamics of irreversible processes[17,18] the water flux is given by

$$q_w = -k\nabla p - S_w \nabla T \tag{9}$$

where k is coefficient of permeability [$m^5/(Js)$] and S_w is a phenomenological coefficient [$m^2/(s^\circ C)$] relating the influence of the thermal gradient on water flux (*thermo-osmosis*). Gravity potential is neglected in equation (9) without loss of generality. In traditional geotechnical engineering applications, the influence of thermo-osmosis is neglected. It has been reported in the literature that the influence of thermo-osmosis can be significant for clay-rich barriers used in radioactive waste containment schemes.[4,20]

Substitution of equation (9) and (1) into equation (8) results in

$$k\nabla^2 p + S_w \nabla^2 T = \xi \frac{\partial u_{j,j}}{\partial t} - c_1 \frac{\partial T}{\partial t} + c_2 \frac{\partial p}{\partial t} \tag{10}$$

where

$$c_1 = n\alpha_w + (1-n)\alpha_s - \frac{\alpha K'}{K_s}, \qquad c_2 = \frac{n}{\beta_w} + \frac{1-n}{K_s} \tag{11}$$

For a medium with incompressible constituents, $\xi = 1$ and $c_2 = 0$. If thermal expansion of constituents are also negligible then $c_1 = 0$. The porosity of the medium generally varies with time under loading. However, in linear models, it is assumed that this variation is sufficiently small that constant n, c_1 and c_2 can be assumed.

Neglecting convection, the total heat flux q_T is given by

$$q_T = -\lambda \nabla T - S_w^* \nabla p \tag{12}$$

where $\lambda (= n\lambda_s + (1-n)\lambda_w$; λ_s and λ_w are thermal conductivities of water and soil grains) is the thermal conductivity of soil (W/m/°C), $S_w^* = (T + T_0)S_w$ is a phenomenological coefficient relating contribution of pressure gradient to the heat flux (thermal filtration), and T_0 is reference temperature.

The heat energy balance equation can be expressed in terms of a single equation of the following form for constituents in thermal equilibrium and for small changes in temperature ($T + T_0 \approx T_0$).

$$C_v \frac{\partial T}{\partial t} - T_0 \alpha_w \beta_w \nabla q_w - T_0 K' \alpha \frac{\partial \varepsilon_v}{\partial t} = -\nabla q_T \tag{13}$$

where C_v is the volumetric specific heat of the soil medium (J/m^3/°C).

The first term on the left-hand side of equation (13) represents the rate of internal heat energy change per unit volume, the second term approximates the heat sink due to thermal dilatation of the fluid and the third term the heat sink due to thermal expansion of the medium.[23]

The substitution of equations (9) and (12) into equation (13) yields

$$C_v \frac{\partial T}{\partial t} - T_0 K' \alpha \frac{\partial \varepsilon_v}{\partial t} = (\lambda - T_0 \alpha_w \beta_w S_w) \nabla^2 T + T_0 (S_w - \alpha_w \beta_w k) \nabla^2 p \tag{14}$$

Application of Laplace transform to equations (3), (10) and (14) with zero initial conditions results in

$$\frac{1-v}{1-2v} 2G \nabla^2 \bar{\varepsilon}_v - \xi \nabla^2 \bar{p} - K' \alpha \nabla^2 \bar{T} = 0 \tag{15}$$

$$k \nabla^2 \bar{p} + S_w \nabla^2 \bar{T} = \xi s \bar{\varepsilon}_v - c_1 s \bar{T} + c_2 s \bar{p} \tag{16}$$

$$C_v s \bar{T} - T_0 K' \alpha s \bar{\varepsilon}_v = (\lambda - T_0 \alpha_w \beta_w S_w) \nabla^2 \bar{T} + T_0 (S_w - \alpha_w \beta_w k) \nabla^2 \bar{p} \tag{17}$$

where s is the Laplace transform variable, and an overbar ($\bar{}$) is hereafter used to denote the Laplace transform of a given variable. All material constants in the above governing equations are assumed to be constants.

RADIALLY SYMMETRIC SOLUTIONS

General solution

This section derives the general solution of equations (15)–(17) for problems possessing radial symmetry. A cylindrical co-ordinate system (r, θ, z) as shown in Figure 1 is used. The basic unknowns u_r, p and T are functions of only the radial co-ordinate r and plane strain conditions are assumed ($\varepsilon_{rz}, \varepsilon_{\theta z}, \varepsilon_{zz} = 0$).

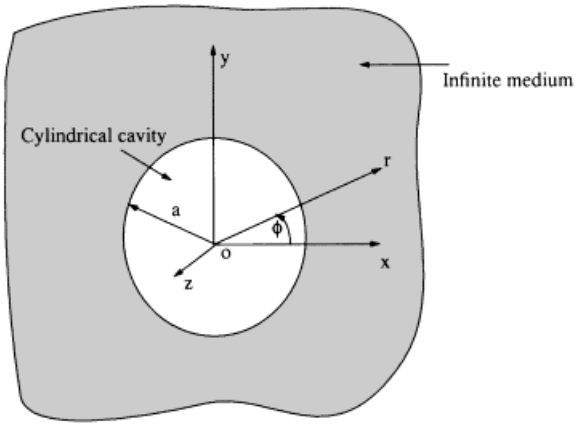

Figure 1. Cylindrical cavity in an infinite medium and the co-ordinate system

From equation (16),

$$\bar{\varepsilon}_{\mathrm{v}} = \frac{S_{\mathrm{w}}}{\xi s}\nabla^2\bar{T} + \frac{k}{\xi s}\nabla^2\bar{p} + \frac{c_1}{\xi}\bar{T} - \frac{c_2}{\xi}\bar{p} \tag{18}$$

where

$$\nabla^2 = \frac{\partial^2}{\partial r^2} + \frac{1}{r}\frac{\partial}{\partial r} \tag{19}$$

Substitution of equation (18) into equation (17) results in

$$a_1\nabla^2\bar{T} + a_2\nabla^2\bar{p} + a_3 s\bar{T} + a_4 s\bar{p} = 0 \tag{20}$$

where

$$a_1 = -\frac{T_0 K'\alpha S_{\mathrm{w}}}{\xi} - \lambda + T_0\alpha_{\mathrm{w}}\beta_{\mathrm{w}}S_{\mathrm{w}}$$

$$a_2 = -\frac{T_0 K'\alpha k}{\xi} - T_0(S_{\mathrm{w}} - \alpha_{\mathrm{w}}\beta_{\mathrm{w}}k)$$

$$a_3 = -\frac{T_0 K'\alpha c_1}{\xi} + C_v, \qquad a_4 = \frac{T_0 K'\alpha c_2}{\xi} \tag{21}$$

Integration of equation (15) results in

$$\frac{1-v}{1-2v}2G\bar{\varepsilon}_{\mathrm{v}} - \xi\bar{p} - K'\alpha\bar{T} = d_1\ln r + d_2 \tag{22}$$

where d_1 and d_2 are unknown constants to be determined from the boundary conditions and the equilibrium equation.

Substitution of equation (18) into equation (22) results in

$$b_1\nabla^2\bar{T} + b_2\nabla^2\bar{p} + b_3 s\bar{T} + b_4 s\bar{p} = s(d_1\ln r + d_2) \tag{23}$$

where

$$b_1 = \frac{2(1-v)GS_w}{(1-2v)\xi}, \qquad b_2 = \frac{2(1-v)Gk}{(1-2v)\xi}$$

$$b_3 = \frac{2(1-v)Gc_1}{(1-2v)\xi} - K'\alpha, \qquad b_4 = -\frac{2(1-v)Gc_2}{(1-2v)\xi} - \xi \tag{24}$$

In the absence of thermodynamically coupled flows, $b_1 = 0$. If thermal expansion of constituents are neglected then $b_3 = 0$. Under these conditions temperature and pore pressure are uncoupled, and the temperature is governed by the classical diffusion equation.

Manipulation of equation (20) and equation (23) results in

$$\bar{T} = -\frac{a_1b_2 - b_1a_2}{(a_1b_3 - a_3b_1)s}\nabla^2\bar{p} - \frac{a_1b_4 - b_1a_4}{a_1b_3 - a_3b_1}\bar{p} + \frac{a_1(d_1 \ln r + d_2)}{(a_1b_3 - a_3b_1)} \tag{25}$$

Substitution of equation (25) in equation (20) yields

$$g_1\nabla^4\bar{p} + g_2s\nabla^2\bar{p} + g_3s^2\bar{p} + \frac{a_3s^2(d_1 \ln r + d_2)}{(a_1b_3 - a_3b_1)} = 0 \tag{26}$$

where

$$g_1 = -\frac{a_1b_2 - b_1a_2}{a_1b_3 - a_3b_1}, \qquad g_2 = \frac{a_2}{a_1} - \frac{a_1b_4 - b_1a_4}{a_1b_3 - a_3b_1} - \frac{a_3}{a_1}\frac{a_1b_2 - b_1a_2}{(a_1b_3 - a_3b_1)}$$

$$g_3 = \frac{a_4}{a_1} - \frac{a_1b_4 - b_1a_4}{a_1b_3 - a_3b_1}\frac{a_3}{a_1} \tag{27}$$

Equation (26) can be rewritten as

$$(\nabla^2 - s\gamma_1^2)(\nabla^2 - s\gamma_2^2)\bar{p} + \frac{a_3s^2(d_1 \ln r + d_2)}{g_1(a_1b_3 - a_3b_1)} = 0 \tag{28}$$

where

$$\gamma_1^2 = \frac{-g_2 - \sqrt{(g_2^2 - 4g_1g_3)}}{2g_1}, \qquad \gamma_2^2 = \frac{-g_2 + \sqrt{(g_2^2 - 4g_1g_3)}}{2g_1} \tag{29}$$

The general solution of equation (28) is

$$\bar{p} = A_1I_0(\gamma_1\sqrt{sr}) + B_1K_0(\gamma_1\sqrt{sr}) + A_2I_0(\gamma_2\sqrt{sr}) + B_2K_0(\gamma_2\sqrt{sr}) + h_0(d_1 \ln r + d_2), \quad Re(\gamma_1, \gamma_2 > 0) \tag{30}$$

where A_1, A_2, B_1 and B_2 are arbitrary functions to be determined from the boundary conditions.

Using equation (30) and equation (25),

$$\bar{T} = (h_1\gamma_1^2 + h_2)[A_1I_0(\gamma_1\sqrt{sr}) + B_1K_0(\gamma_1\sqrt{sr})] + (h_1\gamma_2^2 + gh_2)[A_2I_0(\gamma_2\sqrt{sr}) + B_2K_0(\gamma_2\sqrt{sr})] + (h_0h_2 + h_3)(d_1 \ln r + d_2) \tag{31}$$

where

$$h_0 = -\frac{a_3}{g_3(a_1b_3 - a_3b_1)}, \qquad h_1 = -\frac{a_1b_2 - b_1a_2}{a_1b_3 - a_3b_1}$$

$$h_2 = -\frac{a_1b_4 - b_1a_4}{a_1b_3 - a_3b_1}, \qquad h_3 = \frac{a_1}{(a_1b_3 - a_3b_1)} \tag{32}$$

Substitution of equations (30) and (31) in equation (22) results in

$$\bar{\varepsilon}_v = E_1A_1I_0(\gamma_1\sqrt{sr}) + E_1B_1K_0(\gamma_1\sqrt{sr}) + E_2A_2I_0(\gamma_2\sqrt{sr}) + E_2B_2K_0(\gamma_2\sqrt{sr}) + M(d_1 \ln r + d_2) \tag{33}$$

where

$$E_1 = [\xi + K'\alpha(h_1\gamma_1^2 + h_2)]/\left(\frac{1-v}{1-2v}2G\right)$$

$$E_2 = [\xi + K'\alpha(h_1\gamma_2^2 + h_2)]/\left(\frac{1-v}{1-2v}2G\right)$$

$$M = [1 + \xi h_0 + K'\alpha(h_0h_2 + h_3)]/\left(\frac{1-v}{1-2v}2G\right) \tag{34}$$

Introduce a displacement potential function $\psi(r, t)$ such that

$$u_r = \frac{\partial\psi}{\partial r} \tag{35}$$

Then from equation (33),

$$\nabla^2\bar{\psi} = E_1A_1I_0(\gamma_1\sqrt{sr}) + E_1B_1K_0(\gamma_1\sqrt{sr}) + E_2A_2I_0(\gamma_2\sqrt{sr}) + E_2B_2K_0(\gamma_2\sqrt{sr}) + M(d_1 \ln r + d_2) \tag{36}$$

The general solution of equation (36) is

$$\bar{\psi} = \frac{E_1A_1}{s\gamma_1^2}I_0(\gamma_1\sqrt{sr}) + \frac{E_1B_1}{s\gamma_1^2}K_0(\gamma_1\sqrt{sr}) + \frac{E_2A_2}{s\gamma_2^2}I_0(\gamma_2\sqrt{sr}) + \frac{E_2B_2}{s\gamma_2^2}K_0(\gamma_2\sqrt{sr}) + \frac{M}{4}[d_1r^2(\ln r - 1) + d_2r^2] + d_3 \ln r + d_4 \tag{37}$$

The solution for radial displacement and stresses σ_{rr} and $\sigma_{\theta\theta}$ can then be expressed as

$$\bar{u}_r = \frac{E_1A_1}{\sqrt{s\gamma_1}}I_1(\gamma_1\sqrt{sr}) - \frac{E_1B_1}{\sqrt{s\gamma_1}}K_1(\gamma_1\sqrt{sr}) + \frac{E_2A_2}{\sqrt{s\gamma_2}}I_1(\gamma_2\sqrt{sr}) - \frac{E_2B_2}{\sqrt{s\gamma_2}}K_1(\gamma_2\sqrt{sr}) + \frac{M}{4}[d_1r(2 \ln r - 1) + 2d_2r] + \frac{d_3}{r} \tag{38}$$

$$\bar{\sigma}_{rr} = -2G\left\{\frac{E_1A_1I_1(\gamma_1\sqrt{sr})}{\gamma_1\sqrt{sr}} - \frac{E_1B_1K_1(\gamma_1\sqrt{sr})}{\gamma_1\sqrt{sr}} + \frac{E_2A_2I_1(\gamma_2\sqrt{sr})}{\gamma_2\sqrt{sr}} - \frac{E_2B_2K_1(\gamma_2\sqrt{sr})}{\gamma_2\sqrt{sr}} + \frac{M}{4}[d_1(2\ln r - 1) + 2d_2] + \frac{d_3}{r^2}\right\} + d_1\ln r + d_2 \tag{39}$$

$$\bar{\sigma}_{\theta\theta} = -2G\left\{E_1A_1\left[I_0(\gamma_1\sqrt{sr}) - \frac{I_1(\gamma_1\sqrt{sr})}{\gamma_1\sqrt{sr}}\right] + E_1B_1\left[K_0(\gamma_1\sqrt{sr}) + \frac{K_1(\gamma_1\sqrt{sr})}{\gamma_1\sqrt{sr}}\right] + E_2A_2\left[I_0(\gamma_2\sqrt{sr}) - \frac{I_1(\gamma_2\sqrt{sr})}{\gamma_2\sqrt{sr}}\right] + E_2B_2\left[K_0(\gamma_2\sqrt{sr}) + \frac{K_1(\gamma_2\sqrt{sr})}{\gamma_2\sqrt{sr}}\right] + \frac{M}{4}[d_1(2\ln r + 1) + 2d_2] - \frac{d_3}{r^2}\right\} + d_1\ln r + d_2 \tag{40}$$

Since equation (3) has been used to derive the above solutions instead of equation (2), the following equilibrium equation is also used to determine the unknown coefficients in addition to the boundary/continuity conditions.

$$\frac{\partial\sigma_{rr}}{\partial r} + \frac{\sigma_{rr} - \sigma_{\theta\theta}}{r} = 0 \tag{41}$$

Substitution of equations (39) and (40) into equation (41) results in

$$d_1 = 0 \tag{42}$$

The remaining six arbitrary coefficients (A_1, A_2, B_1, B_2, d_2 and d_3) are determined from the boundary/continuity conditions.

Cylindrical cavity in an infinite medium

The case of a saturated medium with a long cylindrical cavity of radius 'a' is considered (Figure 1). The cavity surface is subjected to a known temperature increase $T_1(t)$. The boundary and initial conditions can be expressed as

$$\sigma_{rr}(a, t) = 0, \qquad p(a, t) = 0, \qquad T(a, t) = T_1(t) \tag{43}$$

$$\sigma_{rr}(r, 0) = 0, \qquad p(r, 0) = 0, \qquad T(r, 0) = 0 \tag{44}$$

Note that alternate boundary conditions such as $u_r(a, t) = 0$ and/or $q_{wr}(a, t) = 0$, where q_{wr} is the radial water flux, can be considered without difficulty. It is not necessary to assume stress free conditions at $r = a$ in equation (43). Specified loading can also be considered.

Equation (43) can be expressed in the Laplace transform domain as

$$\bar{\sigma}_{rr}(a, t) = 0 \qquad \bar{p}(a, t) = 0, \qquad \bar{T}(a, t) = \bar{T}_1 \tag{45}$$

where $\bar{T}_1$ is the Laplace transform of $T_1(t)$.

The general solution of an infinite medium satisfying regularity of variables at $r \to \infty$ is given by equations (30), (31) and (38) with the following condition:

$$A_1 \equiv A_2 \equiv d_2 \equiv 0 \tag{46}$$

Substitution of equations (30), (31) and (39) in equations (45) results in the following solutions for the remaining arbitrary functions:

$$B_1 = \frac{\bar{T}_1}{h_1(\gamma_1^2 - \gamma_2^2)K_0(\gamma_1\sqrt{sa})}$$

$$B_2 = -\frac{\bar{T}_1}{h_1(\gamma_1^2 - \gamma_2^2)K_0(\gamma_2\sqrt{sa})}$$

$$d_3 = a\bar{T}_1\left[\frac{E_1K_1(\gamma_1\sqrt{sa})}{h_1\gamma_1(\gamma_1^2 - \gamma_2^2)s^{1/2}K_0(\gamma_1\sqrt{sa})} - \frac{E_2K_1(\gamma_2\sqrt{sa})}{h_1\gamma_2(\gamma_1^2 - \gamma_2^2)s^{1/2}K_0(\gamma_2\sqrt{sa})}\right] \tag{47}$$

Equations (30), (31), (38)–(40) together with equations (42), (46) and (47) constitute the complete solution in the Laplace domain. The inversion of Laplace transform is complicated due to the presence of modified Bessel functions. A closed form time-domain solution cannot be obtained even in the case where temperature increase is given by a step function. Therefore, a numerical Laplace inversion scheme is used to obtain time-domain solutions. There are several numerical Laplace inversion schemes reported in literature.[24] The present study uses the following scheme proposed by Stehfest:[25]

$$f(t) \approx \frac{\ln 2}{t}\sum_{n=1}^{N}\zeta_n\bar{f}\left(n\frac{\ln 2}{t}\right) \tag{48}$$

where $\bar{f}$ is the Laplace transform of $f(t)$ and the coefficient ζ_n is given by

$$\zeta_n = (-1)^{n+N/2}\sum_{k=[(n+1)/2]}^{\min(n, N/2)}\frac{k^{N/2}(2k)!}{(N/2-k)!k!(k-1)!(n-k)!(2k-n)!} \tag{49}$$

N is even and is typically in the range of 6–10.

Cylindrical cavity in a non-homogeneous medium

The case of a cylindrical cavity in a non-homogeneous medium is solved next by using the general solutions given above. As an example, consider a cylindrical cavity in an infinite domain consisting of two different materials such as the case of a clay barrier and a host rock (Figure 2).

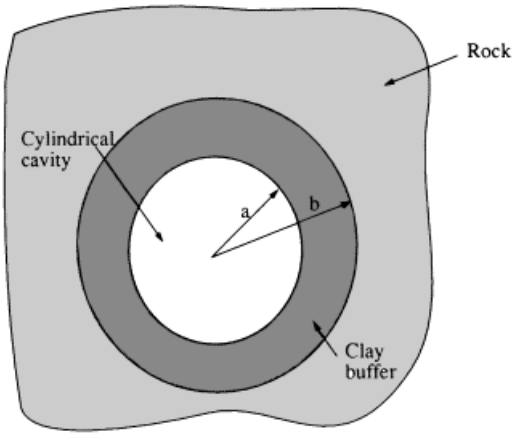

Figure 2. Cylindrical cavity in a non-homogeneous medium

This is a two-domain problem and the general solution of each domain is given by equations (30), (31) and (38)–(40). A superscript i ($i = 1, 2$) is used to denote the field variables and arbitrary coefficients corresponding to each domain. The boundary and continuity conditions can be expressed as,

$$\begin{aligned}
&\bar{\sigma}_{rr}^{(1)}(a,t) = 0, && \bar{p}^{(1)}(a,t) = 0, && \bar{T}^{(1)}(a,t) = \bar{T}_1,\\
&\bar{u}_r^{(1)}(b,t) = \bar{u}_r^{(2)}(b,t), && \bar{p}^{(1)}(b,t) = \bar{p}^{(2)}(b,t), && \bar{T}^{(1)}(b,t) = \bar{T}^{(2)}(b,t)\\
&\bar{\sigma}_{rr}^{(1)}(b,t) = \bar{\sigma}_{rr}^{(2)}(b,t), && \bar{q}_{w_r}^{(1)}(b,t) = \bar{q}_{w_r}^{(2)}(b,t), && \bar{q}_{T_r}^{(1)}(b,t) = \bar{q}_{T_r}^{(2)}(b,t)
\end{aligned} \tag{50}$$

where q_{T_r} denotes the heat flow in the radial direction.

The solution for domain '1' ($a \leqslant r \leqslant b$) involves six arbitrary coefficients ($A_1^{(1)}$, $A_2^{(1)}$, $B_1^{(1)}$, $B_2^{(1)}$, $d_2^{(1)}$, and $d_3^{(1)}$) and that of domain '2' ($b \leqslant r < \infty$) involves only three arbitrary coefficients ($B_1^{(2)}$, $B_2^{(2)}$ and $d_3^{(2)}$). These nine coefficients can be determined from the nine boundary and continuity conditions in equation (50). Other boundary conditions can be considered at $r = a$ without difficulty. Time-domain solutions are obtained by determining the arbitrary coefficients from equation (50) for discrete values of the Laplace transform variable 's' and then using equation (48) for inversion.

SPHERICALLY SYMMETRIC SOLUTION

General solution

This section considers problems possessing spherical symmetry. The analysis uses the sperical co-ordinate system (R, θ, ϕ) shown in Figure 3. All field variables are functions only of co-ordinate R. Equations (2), (10) and (14) can be solved by using a procedure similar to that used for radially symmetric problems. The following general solutions are obtained in the

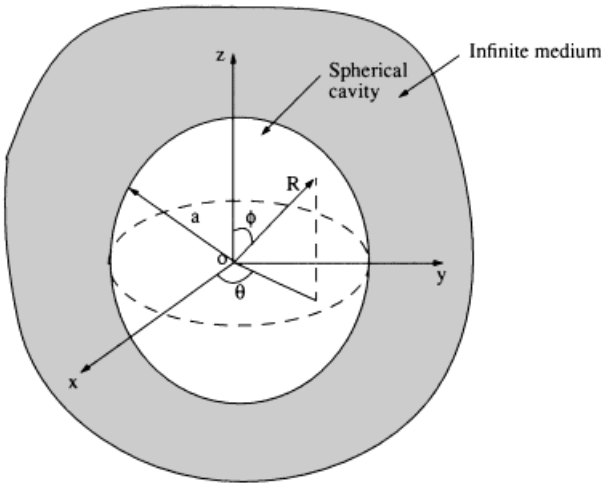

Figure 3. Spherical cavity in an infinite medium and the co-ordinate system

Laplace domain:

$$\bar{p} = A_1 \frac{e^{-\gamma_1\sqrt{sR}}}{R} + B_1 \frac{e^{\gamma_1\sqrt{sR}}}{R} + A_2 \frac{e^{-\gamma_2\sqrt{sR}}}{R} + B_2 \frac{e^{\gamma_2\sqrt{sR}}}{R} + h_0 d_2 \tag{51}$$

$$\bar{T} = (h_1\gamma_1^2 + h_2)\left(A_1 \frac{e^{-\gamma_1\sqrt{sR}}}{R} + B_1 \frac{e^{\gamma_1\sqrt{sR}}}{R}\right) + (h_1\gamma_2^2 + h_2)\left(A_2 \frac{e^{-\gamma_2\sqrt{sR}}}{R} + B_2 \frac{e^{\gamma_2\sqrt{sR}}}{R}\right) + (h_0 h_2 + h_3) d_2 \tag{52}$$

$$\begin{aligned}\bar{u}_R = & -\frac{E_1 A_1}{\sqrt{s\gamma_1}} \frac{e^{-\gamma_1\sqrt{sR}}}{R}\left(1 + \frac{1}{\sqrt{s\gamma_1 R}}\right) + \frac{E_1 B_1}{\sqrt{s\gamma_1}} \frac{e^{\gamma_1\sqrt{sR}}}{R}\left(1 - \frac{1}{\sqrt{s\gamma_1 R}}\right) \\ & - \frac{E_2 A_2}{\sqrt{s\gamma_2}} \frac{e^{-\gamma_2\sqrt{sR}}}{R}\left(1 + \frac{1}{\sqrt{s\gamma_2 R}}\right) + \frac{E_2 B_2}{\sqrt{s\gamma_2}} \frac{e^{\gamma_2\sqrt{sR}}}{R}\left(1 - \frac{1}{\sqrt{s\gamma_2 R}}\right) \\ & + M\frac{d_2}{3} R + \frac{d_3}{R^2}\end{aligned} \tag{53}$$

$$\begin{aligned}\bar{\sigma}_{RR} = 4G\Bigg[& \frac{E_1 A_1}{\sqrt{s\gamma_1}} \frac{e^{-\gamma_1\sqrt{sR}}}{R^2}\left(1 + \frac{1}{\sqrt{s\gamma_1 R}}\right) - \frac{E_1 B_1}{\sqrt{s\gamma_1}} \frac{e^{\gamma_1\sqrt{sR}}}{R^2}\left(1 - \frac{1}{\sqrt{s\gamma_1 R}}\right) \\ & + \frac{E_2 A_2}{\sqrt{s\gamma_2}} \frac{e^{-\gamma_2\sqrt{sR}}}{R^2}\left(1 + \frac{1}{\sqrt{s\gamma_2 R}}\right) - \frac{E_2 B_2}{\sqrt{s\gamma_2}} \frac{e^{\gamma_2\sqrt{sR}}}{R^2}\left(1 - \frac{1}{\sqrt{s\gamma_2 R}}\right) - M\frac{d_2}{3} - \frac{d_3}{R^3}\Bigg] + d_2\end{aligned} \tag{54}$$

$$\bar{\sigma}_{\theta\theta} = -\frac{\bar{\sigma}_{RR}}{2} - 2G\left[E_1\left(A_1\frac{e^{-\gamma_1\sqrt{sR}}}{R} + B_1\frac{e^{\gamma_1\sqrt{sR}}}{R}\right) + E_2\left(A_2\frac{e^{-\gamma_2\sqrt{sR}}}{R} + B_2\frac{e^{\gamma_2\sqrt{sR}}}{R}\right) + Md_2\right] + \frac{3}{2}d_2 \tag{55}$$

where E_1, E_2 and M are given by equation (34). A_1, B_1, A_2, B_2, d_2 and d_3 are arbitrary functions to be determined from boundary and continuity conditions.

Spherical cavity in an infinite medium

Equations (51)–(55) are now used to solve the case of a spherical cavity in an infinite medium subjected to specified thermal, fluid and mechanical loads. The boundary and initial conditions can be expressed as

$$\sigma_{RR}(a, t) = -\sigma_0(t), \quad p(a, t) = p_0(t), \quad T(a, t) = T_1(t), \quad t > 0 \tag{56}$$

$$\sigma_{RR}(R, 0) = 0, \quad p(R, 0) = 0, \quad T(R, 0) = 0 \tag{57}$$

Equation (56) can be expressed in the Laplace transform space as

$$\bar{\sigma}_{RR}(a, t) = -\bar{\sigma}_0, \quad \bar{p}(a, t) = \bar{p}_0, \quad \bar{T}(a, t) = \bar{T}_1 \tag{58}$$

Consideration of regularity conditions of field variables at $R \to \infty$ yields

$$B_1 \equiv B_2 \equiv d_2 \equiv 0 \tag{59}$$

Substitution of equations (51), (52) and (54) in equations (58) results in

$$A_1 = \omega_1 e^{\sqrt{s}\gamma_1 a}$$

$$A_2 = \omega_2 e^{\sqrt{s}\gamma_2 a}$$

$$d_3 = \frac{\bar{\sigma}_0}{4G}a^3 + \frac{E_1\omega_1}{\sqrt{s}\gamma_1}\left(a + \frac{1}{\sqrt{s}\gamma_1}\right) + \frac{E_2\omega_2}{\sqrt{s}\gamma_2}\left(a + \frac{1}{\sqrt{s}\gamma_2}\right) \tag{60}$$

where

$$\omega_1 = -\frac{a[\bar{T}_1 - (h_1\gamma_2^2 + h_2)\bar{p}_0]}{h_1(\gamma_2^2 - \gamma_1^2)}, \qquad \omega_2 = \frac{a[\bar{T}_1 - (h_1\gamma_1^2 + h_2)\bar{p}_0]}{h_1(\gamma_2^2 - \gamma_1^2)} \tag{61}$$

If $T_1, p_0 = 0$, then the solution is identical to the classical ideal elasticity solution. This suggests that mechanical pressurization of a spherical cavity will not induce pore pressure similar to the case of a radially pressurized cylindrical cavity.[26] It is not possible to obtain a closed form time-domain solution for arbitrary time-dependent boundary conditions at $r = a$. The numerical inversion scheme given by equation (48) together with equations (51)–(55), (59) and (60) are used to obtain time-domain solutions.

If $\sigma_0(t) = \sigma_0 H(t)$, $p_0(t) = p_0 H(t)$ and $T_1(t) = T_1 H(t)$, where $H(t)$ is a unit step function, the following closed form time-domain solutions can be obtained:

$$p = \omega_{10} \operatorname{erfc}\left(\frac{\gamma_1(R-a)}{2\sqrt{t}}\right) + \omega_{20} \operatorname{erfc}\left(\frac{\gamma_2(R-a)}{2\sqrt{t}}\right) \tag{62}$$

$$T = (h_1\gamma_1^2 + h_2)\omega_{10} \operatorname{erfc}\left(\frac{\gamma_1(R-a)}{2\sqrt{t}}\right) + (h_1\gamma_2^2 + h_2)\omega_{20} \operatorname{erfc}\left(\frac{\gamma_2(R-a)}{2\sqrt{t}}\right) \tag{63}$$

$$\begin{aligned} u_R = &- \frac{E_1\omega_{10}}{\gamma_1 R}\left\{2\sqrt{\frac{t}{\pi}}\,\mathrm{e}^{-(\gamma_1^2(R-a)^2)/4t} - \gamma_1(R-a)\operatorname{erfc}\left(\frac{\gamma_1(R-a)}{2\sqrt{t}}\right)\right. \\ &\left. + \frac{4t}{\gamma_1 R}\, i^2 \operatorname{erfc}\left(\frac{\gamma_1(R-a)}{2\sqrt{t}}\right)\right\} \\ &+ \frac{E_2\omega_{20}}{\gamma_2 R}\left\{2\sqrt{\frac{t}{\pi}}\,\mathrm{e}^{-(\gamma_2^2(R-a)^2)/4t} - \gamma_2(R-a)\operatorname{erfc}\left(\frac{\gamma_2(R-a)}{2\sqrt{t}}\right)\right. \\ &\left. + \frac{4t}{\gamma_2 R}\, i^2 \operatorname{erfc}\left(\frac{\gamma_2(R-a)}{2\sqrt{t}}\right)\right\} \\ &- \frac{\sigma_0 a^3}{R^2} - \frac{E_1\omega_{10}}{\gamma_1 R^2}\left(2a\sqrt{\frac{t}{\pi}} + \frac{t}{\gamma_1}\right) - \frac{E_2\omega_{20}}{\gamma_2 R^2}\left(2a\sqrt{\frac{t}{\pi}} + \frac{t}{\gamma_2}\right) \end{aligned} \tag{64}$$

$$\sigma_{RR} = -\frac{4G}{R}\, u_R \tag{65}$$

$$\sigma_{\theta\theta} = -\frac{\sigma_{RR}}{2} - 2G\left[E_1\omega_{10} \operatorname{erfc}\left(\frac{\gamma_1(R-a)}{2\sqrt{t}}\right) + E_2\omega_{20} \operatorname{erfc}\left(\frac{\gamma_2(R-a)}{2\sqrt{t}}\right)\right] \tag{66}$$

where

$$\omega_{10} = -\frac{a[T_1 - (h_1\gamma_2^2 + h_2)p_0]}{h_1(\gamma_2^2 - \gamma_1^2)}, \qquad \omega_{20} = \frac{a[T_1 - (h_1\gamma_1^2 + h_2)p_0]}{h_1(\gamma_2^2 - \gamma_1^2)}$$

$$i^2 \operatorname{erfc}(x) = \frac{1}{4}(2x^2 + 1)\operatorname{erfc}(x) - \frac{x}{2\sqrt{\pi}}\,\mathrm{e}^{-x^2} \tag{67}$$

and $i^n \operatorname{erfc}(x)$ denotes the repeated integral of the complementary error function.[27] In the case of a non-homogeneous medium with a spherical cavity, the solution can be found by considering the boundary conditions at the cavity surface and the continuity conditions at materials interfaces as shown previously for a cylindrical cavity.

RESULTS AND DISCUSSION

This section presents selected numerical results that demonstrate the principal features of the coupled thermoporoelastic response and the significance of the thermodynamically coupled transport processes. Three sets of material properties (materials A, B and C) are used in the

analysis. Due to limited data, the following material properties are assumed to be identical for the three materials:

$$\alpha_w = 3{\cdot}0 \times 10^{-4}{}^{\circ}C^{-1}, \qquad \alpha_s = 3{\cdot}0 \times 10^{-6}{}^{\circ}C^{-1}$$

$$\alpha = 3{\cdot}0 \times 10^{-6}{}^{\circ}C^{-1}, \qquad T_0 = 300\ K$$

$$C_s = 0{\cdot}937(kJ/kg/{}^{\circ}C), \qquad C_w = 4{\cdot}186(kJ/kg/{}^{\circ}C)$$

$$\rho_w = 1000\ kg/m^3, \qquad \rho_s = 2610\ kg/m^3$$

$$\beta_w = 3{\cdot}3\ GPa, \qquad K_s = 59\ GPa$$

$$\lambda_s = 3{\cdot}29\ J/(s\,m\,{}^{\circ}C), \qquad \lambda_w = 0{\cdot}582\ J/(s\,m\,{}^{\circ}C)$$

In addition, for material A[20] (clay)

$$S_w = 2{\cdot}70 \times 10^{-10}\ m^2/(s{}^{\circ}C), \qquad k = 5{\cdot}0 \times 10^{-14}\ m^5/(Js)$$

$$E = 2{\cdot}880\ MPa, \quad v = 0{\cdot}2, \quad n = 0{\cdot}375$$

For material B (relatively impermeable rock)

$$S_w = 0\ m^2/(s{}^{\circ}C), \qquad k = 1{\cdot}0 \times 10^{-16}\ m^5/(Js)$$

$$E = 10^4\ MPa, \quad v = 0{\cdot}15 \quad n = 0{\cdot}01$$

and for material C (relatively permeable rock)

$$S_w = 0\ m^2/(s{}^{\circ}C), \qquad k = 1{\cdot}0 \times 10^{-12}\ m^5/(Js)$$

$$E = 10^4\ MPa, \quad v = 0{\cdot}15, \quad n = 0{\cdot}4$$

The units of k given above are $m^5/(Js)$. This is not the traditional units used in geotechnical literature. It should be noted that $1\ m^5/(Js)$ is equivalent to 10^4 m/s.

The accuracy of numerical Laplace inversion is first investigated by considering the case of a spherical cavity of radius 0·5 m in an infinite medium (material A) subjected to a constant temperature increase of $T_1 = 50{}^{\circ}C$ at the stress free and fully permeable cavity surface. The exact analytical solution in the time-domain is given by equations (62)–(66). The solution for this problem can also be obtained by using equations (51)–(55), (59) and (60) together with the numerical Laplace inversion given by equation (48). Tables I and II presents a comparison between the analytical solution and the solution based on the numerical Laplace inversion scheme with $N = 10$ in equation (48). The two solutions agree closely and confirm the accuracy of the numerical Laplace inversion scheme that has been used. Comparisons were also done with $N = 12$, 14 and 16, and the solutions were in very good agreement with the analytical solutions. In the remainder of the paper, all numerical Laplace inversions were performed with $N = 10$ in equation (48).

Cylindrical cavity in an infinite medium

Figure 4 shows the thermodynamically coupled response of an infinite medium (material A) with a cylindrical borehole of radius $a = 0{\cdot}5$ m subjected to a sudden increase of temperature

Table I. Comparison of numerical and analytical solutions for temperature increase (°C) ($N = 10$)

R	$t = 5$ h		$t = 1000$ h		$t = 50\,000$ h	
	Analy.	Num.	Analy.	Num.	Analy.	Num.
0·5	50·000	50·000	50·000	50·000	50·000	50·000
0·7	7·548	7·544	33·23	33·23	35·36	35·36
1·0	0·416	0·389	29·67	20·67	24·38	24·38
1·5	0·000	0·000	11·02	11·02	15·85	15·85
2·0	0·000	0·000	6·377	6·377	11·58	11·58
3·0	0·000	0·000	2·249	2·248	7·310	7·310
4·0	0·000	0·000	0·757	0·757	5·179	5·179
5·0	0·000	0·000	0·229	0·230	3·904	3·904

Table II. Comparison of numerical and analytical solutions for pore water pressure (kPa) ($N = 10$)

	$t = 5$ h		$t = 1000$ h		$t = 50\,000$ h	
R	Analy.	Num.	Analy.	Num.	Analy.	Num.
0·5	0·000	0·000	0·000	0·000	0·000	0·000
0·7	14·86	14·85	5·511	5·511	0·787	0·787
1·0	0·086	0·081	9·175	9·174	1·375	1·375
1·5	0·000	0·000	10·27	10·27	1·827	1·827
2·0	0·000	0·000	8·721	8·723	2·043	2·043
3·0	0·000	0·000	4·253	4·249	2·228	2·228
4·0	0·000	0·000	1·547	1·548	2·273	2·273
5·0	0·000	0·000	0·474	0·475	2·252	2·252

($T_1 = 50$°C) at the fully permeable and stress free borehole surface. The initial conditions are given by equation (44). The response of an identical medium in the absence of thermodynamically coupled heat–mass flow ($S_w = 0$, also neglecting the heat sink term in equation (13)) is presented in Figure 5 for comparison. Substantial pore water pressures are developed in the medium due to thermodynamically coupled heat–water flow. For example, the maximum pore water pressure in the thermodynamically coupled case is 28 kPa compared to 6·5 kPa in the semi-coupled case. The general shape of pore water pressure isochrones is similar for both cases. Pore pressure due to heating is initially generated near the borehole and propagates radially as time progresses. Pore pressure completely dissipates as $t \to \infty$. This trend is confirmed in Figures 4 and 5 although it would take a very long time to approach zero pressure due to the very low permeability of the medium.

The isochrones of temperature changes shown in Figures 4 and 5 are nearly identical implying that thermo-osmosis and thermal filtration have a negligible influence on temperature increase. It can be shown that the medium experiences a uniform temperature increase of $T_1 = 50$°C as $t \to \infty$. The isochrones for radial displacements in Figures 4 and 5 show substantial differences similar to the case of pore pressure. The instantaneous peak value of radial displacement for the thermodynamically coupled case is much larger than the corresponding solution for the

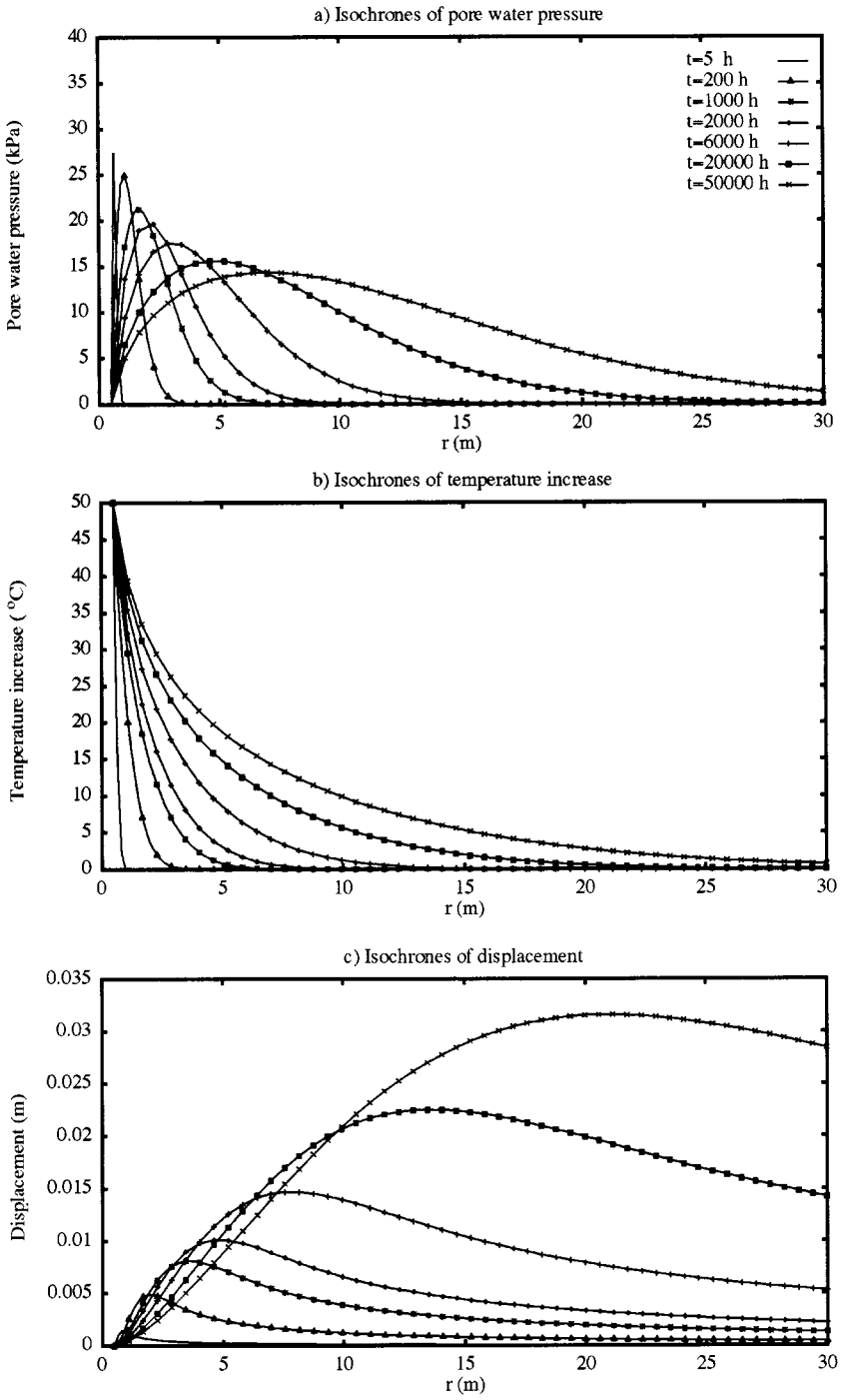

Figure 4. Coupled fields in an infinite medium (material A) due to constant temperature increase ($T = 50°C$) at a cylindrical borehole surface ($a = 0{\cdot}5$ m)

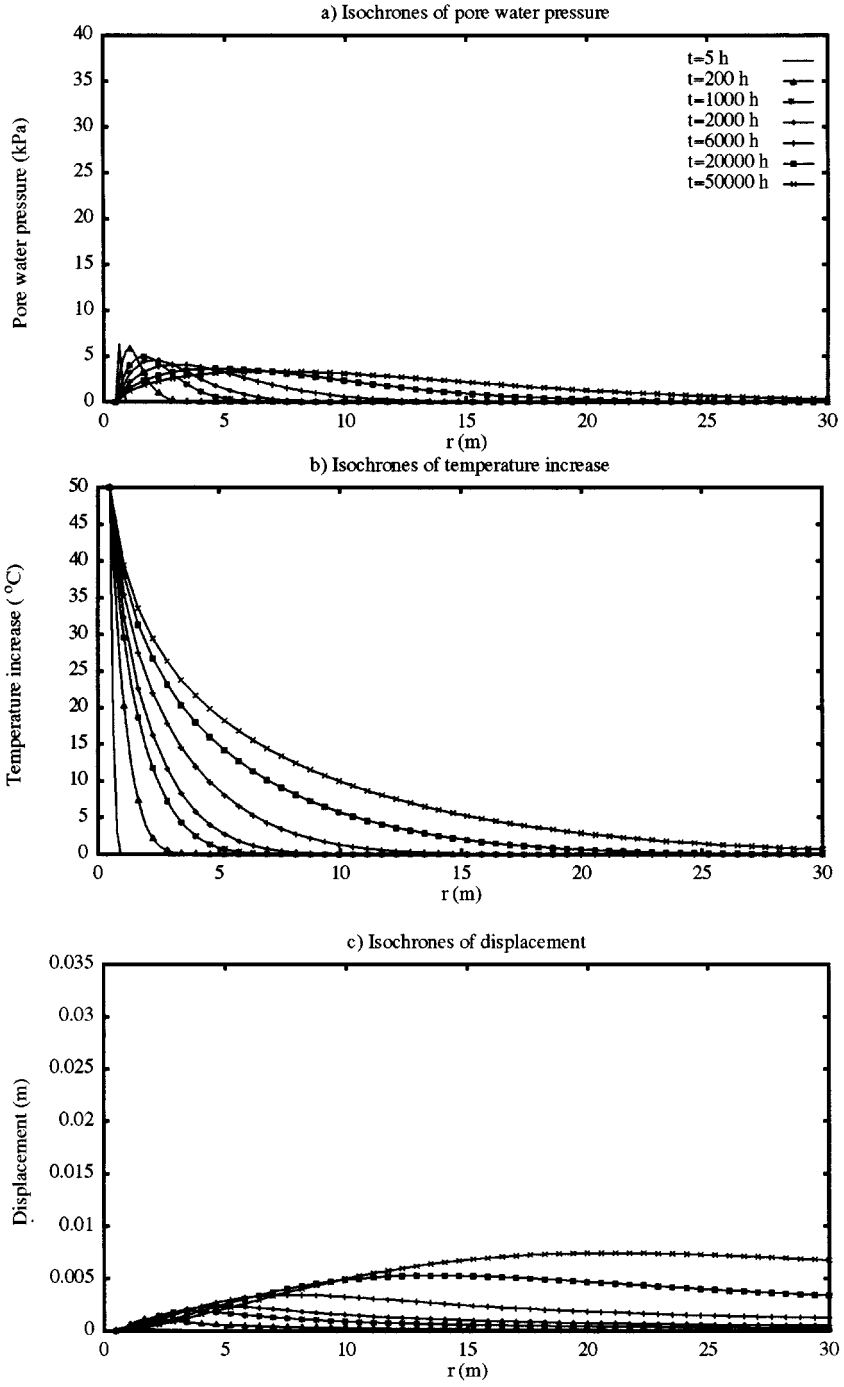

Figure 5. Semi-coupled fields in an infinite medium (material A) due to constant temperature increase ($T = 50°C$) at a cylindrical borehole surface ($a = 0{\cdot}5$ m)

semi-coupled case. Maximum displacement is observed at an interior point. The radial displacement at the borehole surface is zero for both coupled and semi-coupled solutions. A similar situation exists in the case of ideal thermoelasticity.

The displacement at points near the heated wall initially increases with time and then decreases as can be seen in Figures 4 and 5. The initial expansion is due to the heating which generates relatively large pore pressures in the near-field resulting in flow of water away from the near-field which then causes a reduction in the displacement. In the far-field, however, the radial displacement increases with time due to the continuous outward heat flow. It can be shown analytically that as $t \to \infty$ the displacement increases radially resulting in singular displacements as $r \to \infty$. This behaviour is a consequence of the assumed boundary conditions at the cavity surface.

Figure 6 shows thermodynamically coupled fields corresponding to an identical borehole subjected to a temperature increase $T = 50\,\mathrm{e}^{-7{\cdot}0\times10^{-9}t}H(t)$, where t is the elapsed time. This temperature boundary condition may be considered as an approximation for a radioactive waste canister placed in the cavity. Pore pressure isochrones are nearly identical to that in Figure 4 for $t < 6000$ h. Relatively smaller pore pressures are generated in the far-field as time progresses. Temperature isochrones are naturally different from the previous case due to the assumed temperature boundary condition. The temperature decreases to about 4°C at the cavity surface after 100,000 h (approx. 11 yr). Radial displacements isochrones for $t < 6000$ h are nearly identical to those in Figure 4. However, as in the case of pore water pressure, the far-field experiences relatively lower displacements with increasing time. Displacement due to heating is zero at the cavity surface. This condition naturally simulates the large stiffness of a metal canister when compared to a clay buffer.

Instantaneous peak displacements are noted inside the medium as in the previous case. The initial increase of displacement and subsequent reduction is seen over a larger domain ($r < 20$ m) when compared to Figure 4. This is a consequence of the exponentially decaying temperature boundary condition that results in a completely different temperature distribution. Consequently, lower pore pressures are generated in the medium. Lower temperature and pore pressure increases also result in smaller displacements when compared to Figure 4. Both the temperature increase and the radial displacements approach zero as $t \to \infty$. Therefore, the steady-state solution is completely different from those in Figure 4. Solutions for the semi-coupled case ($S_w = 0$ and neglecting the heat sink in equation (13)) with identical boundary conditions were also computed. The results show substantially lower pore water pressures and displacements when compared to the Figure 6.

Cylindrical cavity in a non-homogeneous medium

Coupled fields in non-homogeneous domains as shown in Figure 2 are considered in this section. Figures 7 and 8 show the response of a hollow clay cylinder of material A (inner radius $a = 0{\cdot}5$ m, outer radius $b = 1{\cdot}0$ m) surrounded by an infinite medium of material B or C, respectively. Thermodynamic coupling is neglected for materials B and C ($S_w = 0$). The fully permeable and fixed ($u_r = 0$) inner wall of the clay cylinder is subjected to an exponentially decaying temperature increase $T = 50\,\mathrm{e}^{-7{\cdot}0\times10^{-9}t}H(t)$ simulating a decaying heat source. The inner wall is fixed to simulate the case of a stiff metallic container occupying the inner core. The initial conditions are given by equation (44). Material B is lesser permeable than either material A (clay) or material C. The permeability of material C is representative of that of limestone/sandstone whereas material B is representative of granite. Both materials are assumed to

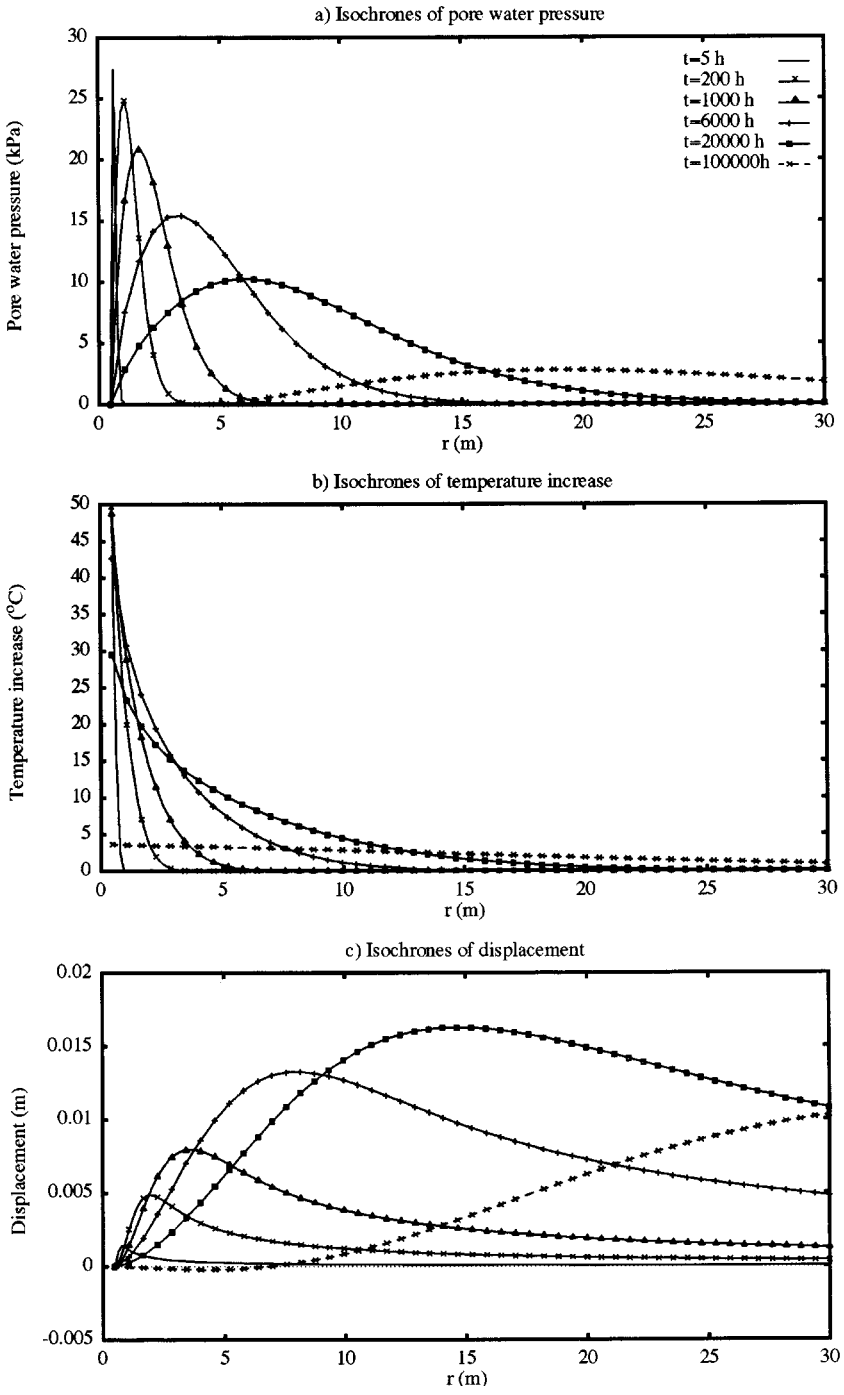

Figure 6. Coupled fields in an infinite medium (material A) due to exponentially decaying temperature increase $[T = 50\exp(-7\times10^{-9}\,t)^{\circ}C]$ at a cylindrical borehole surface ($a = 0{\cdot}5$ m)

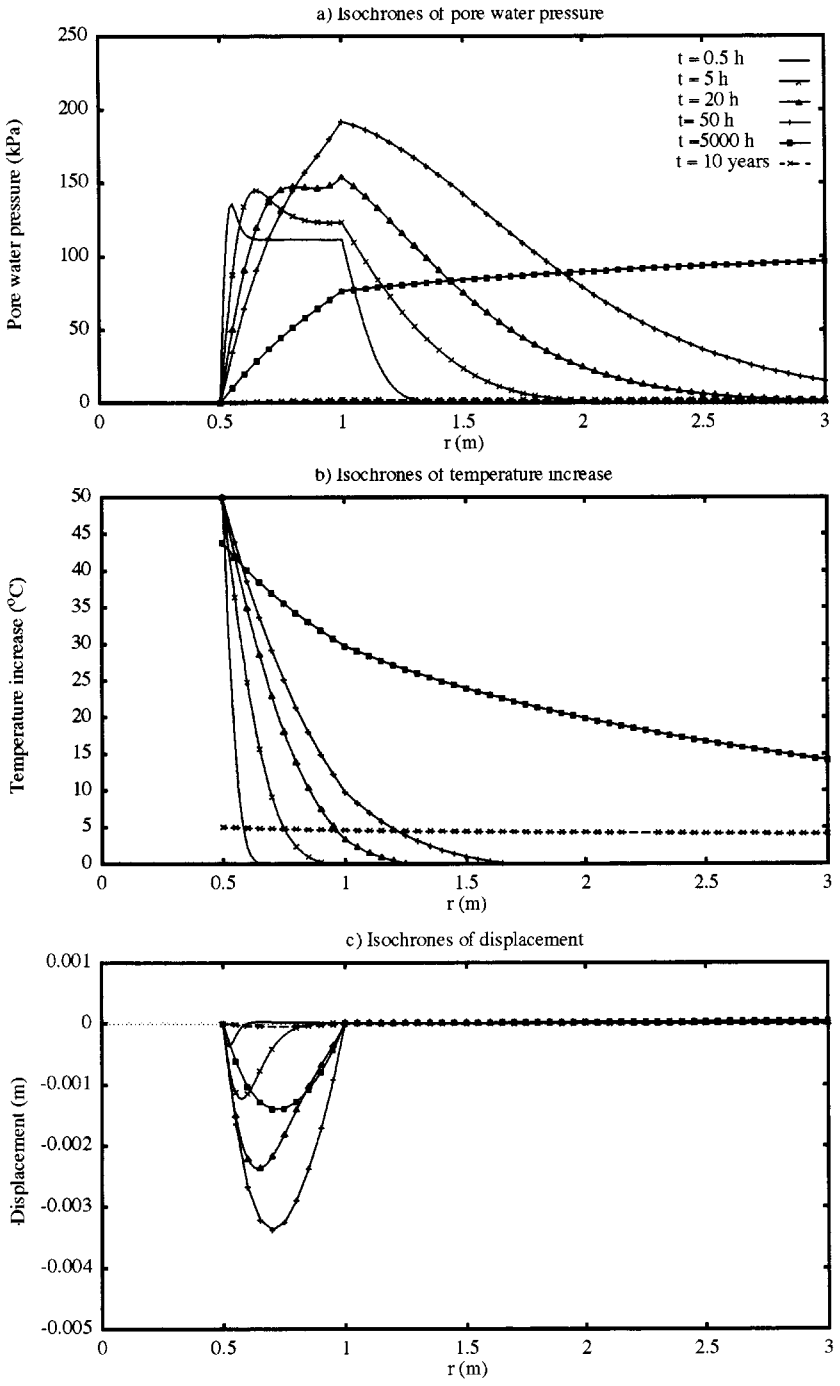

Figure 7. Coupled fields in a non-homogeneous domain (materials A and B) due to exponentially decaying temperature increase [$T = 50\exp(-7\times10^{-9}\,t)$°C] at the inner cavity surface ($a = 0{\cdot}5$ m, $b = 1{\cdot}0$ m)

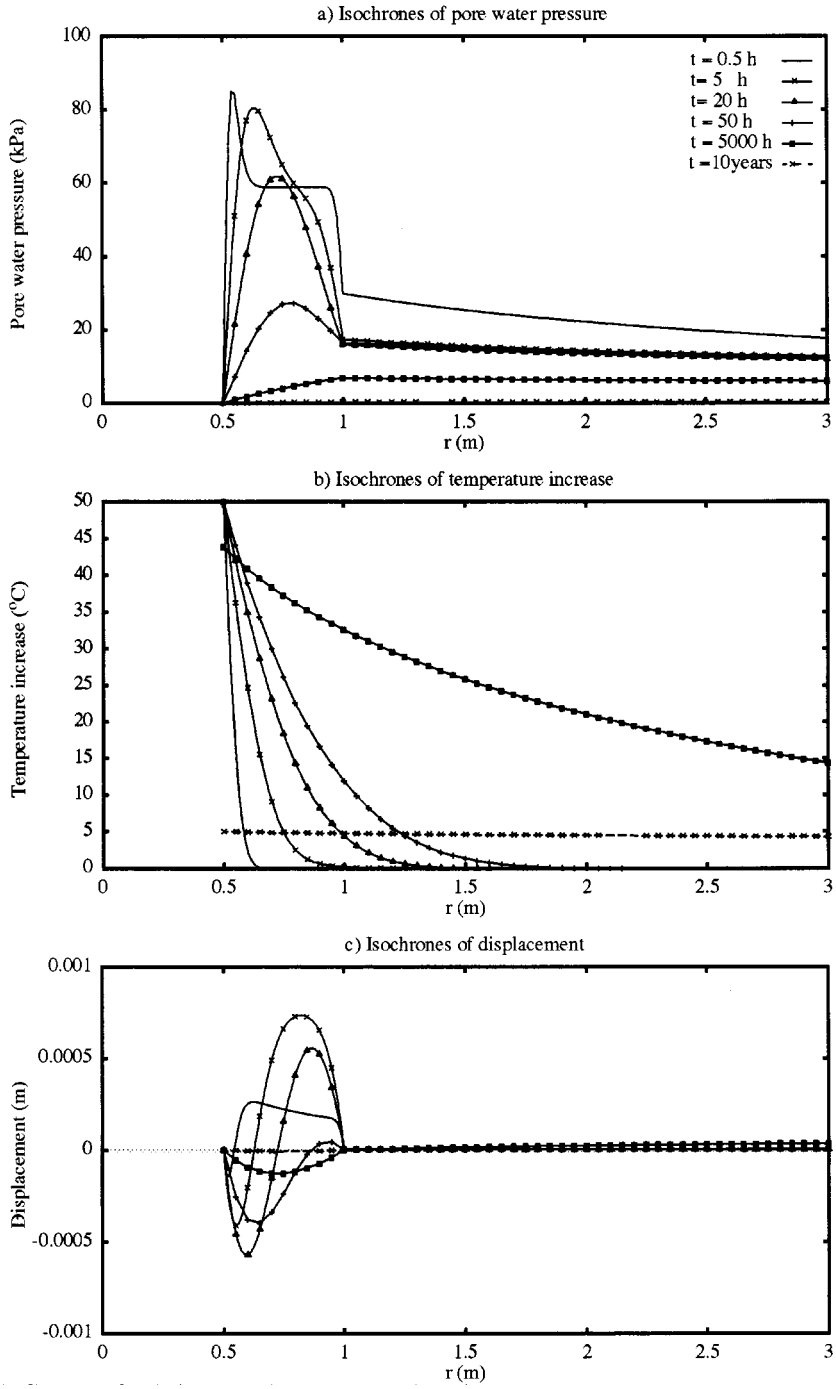

Figure 8. Coupled fields in a non-homogeneous domain (materials A and C) due to exponentially decaying temperature increase $[T = 50\exp(-7\times10^{-9}\,t)^{\circ}C]$ at the inner cavity surface ($a = 0{\cdot}5$ m, $b = 1{\cdot}0$ m)

have identical elastic properties that are substantially stiffer than material A. The two different materials selected for the exterior region allows the investigation of the influence of permeability of a host rock surrounding a clay buffer.

Pore water pressure isochrones in Figures 7 and 8 show substantial increases (over five times in Figure 7) in magnitude when compared to Figure 6 under identical thermal loading. Thus, the presence of a stiffer external medium with a permeability lower or higher than material A results in a significant increase in pore water pressure in the clay buffer which is here 0·5 m thick. The increase in pressure appears to be primarily due to the confinement provided by the stiffer outer medium. This is enhanced by the lower permeability of the outer medium. The results shown in Figures 7 and 8 imply the potential for hydraulic fracture due to thermal loading in a confined environment. Tanaka and Graham[28] observed in their experimental studies the development of large pore pressures in a confined illitic clay sample due to heating. The present results show qualitatively similar behaviour. A discontinuity in the pore pressure isochrone occurs at the material interface due to the difference in permeabilities of inner and outer materials. The peak pore pressure in the outer medium is nearly half of that in the inner clay cylinder. The pore water pressures have nearly dissipated for $t > 10$ yr.

Temperatures isochrones in Figures 7 and 8 are nearly identical. This implies a negligible dependence of temperature on elastic and hydraulic properties of the outer medium. Temperature in the near field reduces to nearly one-tenth of the initial temperature at the cavity wall after ten years. The steady state corresponds to a zero temperature increase. Displacement isochrones in Figures 7 and 8 are substantially different from previous solutions for a homogeneous medium. The displacement of the outer medium ($r > 1$ m) is practically zero for both materials B and C. This is due to the high elastic stiffness of these materials when compared to material A. Since the inner cavity wall is also fixed (simulates the high stiffness of a metal canister) the clay buffer is in a highly confined state. Displacements within the material A is inward in Figure 7 whereas Figure 8 shows both inward and outward displacement with time. Peak displacements are slightly larger in the case of a cylinder surrounded by material C when compared to material B but substantially smaller than the solutions in Figure 4 for a homogeneous medium of material A. The differences between the displacement isochrones in Figures 7 and 8 are primarily due to the difference in permeability of materials B and C. Steady-state displacements are zero.

Spherical cavity in an infinite medium

Figure 9 shows the thermodynamically coupled response of an infinite medium (material A) with a spherical cavity of radius $a = 0{\cdot}5$ m subjected to a sudden increase of temperature ($T_1 = 50^\circ$C) at the fully permeable and stress-free cavity surface. As in the case of a cylindrical cavity, considerable pore water pressures are developed in the near-field at early times. Pore pressures dissipate very slowly due to the very low permeability of the medium.

Isochrones of temperature increase show a rapid decay with distance when compared to the case of a cylindrical cavity. The steady-state temperature distribution is inversely proportional to the distance from the cavity centre and is reached when $t > 20{,}000$ h. However, it takes longer than 100,000 h to compeletely dissipate the pore pressure. Displacement isochrones show zero displacement at the cavity surface similar to the case of a cylindrical cavity. This can also be seen from the analytical solution. Displacements in the near-field initially increase with time and then decrease. This is a consequence of the initial thermal expansion and subsequent water flow due to pore pressure. Displacements are comparatively smaller than those in Figure 4 and the

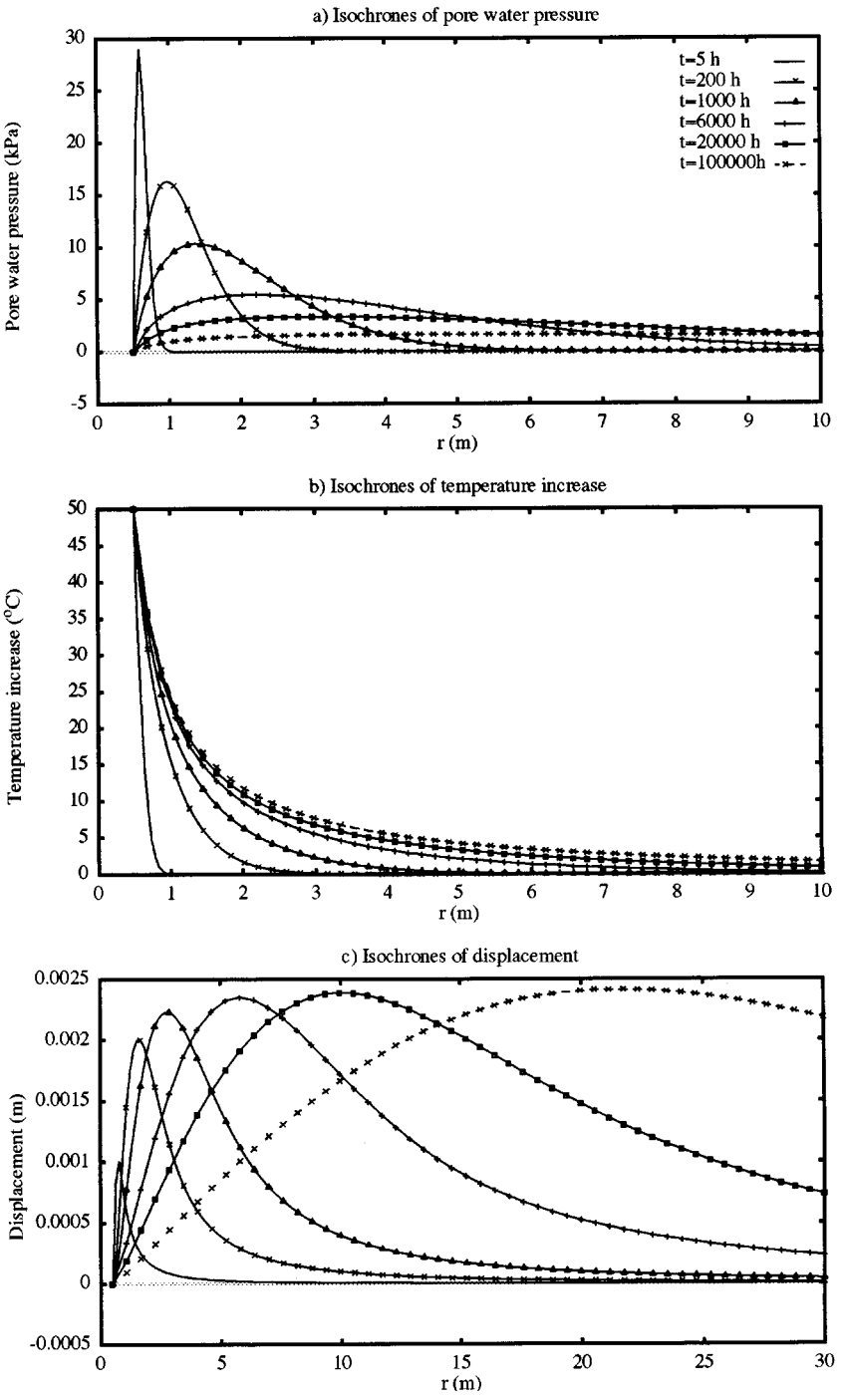

Figure 9. Coupled fields in an infinite medium (material A) due to constant temperature increase ($T = 50°C$) at a spherical cavity surface ($a = 0{\cdot}5$ m)

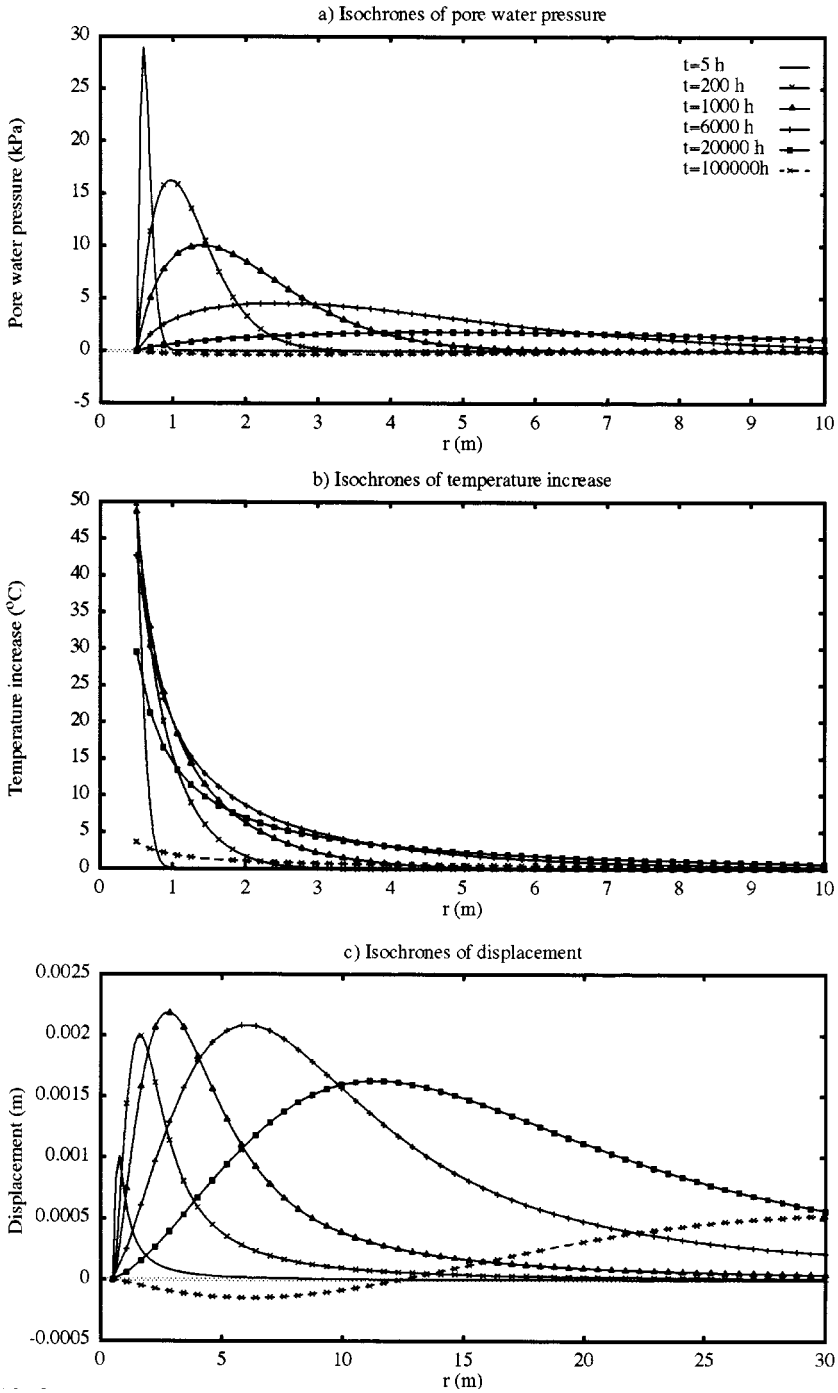

Figure 10. Coupled fields in an infinite medium (material A) due to exponentially decaying temperature increase $[T = 50 \exp(-7 \times 10^{-9} t)°C]$ at a spherical cavity surface ($a = 0{\cdot}5$ m)

steady-state solution is a linear function of the coordinate R. Solutions for the semi-coupled case ($S_w = 0$ and neglecting heat sinks in equation (13)), are similar in shape but the peak pore water pressures and radial displacements are less than one-third of the peak solutions in Figure 9. Temperature isochrones are nearly identical for the semi-coupled and coupled cases.

Figure 10 shows the response of an identical medium subjected to an exponentially decreasing temperature increase $T = 50\,e^{-7{\cdot}0\times10^{-9}t}H(t)$ at the cavity surface. Lower pore water pressures are developed in the medium for $t > 1000$ h when compared to Figure 9. Pore water pressure dissipation is relatively faster in this case and negligible suction is noted when $t = 100{,}000$ h. Temperature isochrones are qualitatively similar to those in Figure 6 and the increase in temperature is mainly confined to $R < 10$ m. Displacements are also smaller but qualitatively similar to those in Figure 9 at early times. The initial swelling due to the temperature increase and subsequent recovery is noted in the near-field as in Figure 9. The displacements at the cavity surface is zero at all times and the near-field experiences a negligible inward displacement when $t > 100{,}000$ h. The steady-state displacement is zero everywhere but it takes a substantially larger time to reach this situation since the pore pressure dissipation is very slow.

CONCLUSIONS

It is shown that analytical solutions can be derived in the Laplace transform domain for linear equations governing radially or spherically symmetric thermoporoelastic fields. The application of Laplace domain solutions is demonstrated by considering cavities in homogeneous and non-homogeneous media. Time-domain solutions are obtained by using a numerical inversion for a cylindrical cavity due to the complexity of the Laplace inversion. Closed form time-domain solutions can be derived for a spherical cavity subjected to uniform mechanical, thermal and fluid loading with a step function time history.

Numerical results indicate that thermodynamically coupled heat and water flow (thermo-osmosis and thermal filtration) result in substantial increases in pore water pressures and displacements due to heating but have a negligible effect on temperature. Semi-coupled models that neglect thermodynamically coupled heat and water flow result in smaller pore water pressures and displacements. In the case of non-homogeneous domains, the presence of a stiffer outer domain with a lower permeability results in substantially higher pore pressures while temperature distribution is almost unchanged from a homogeneous medium with properties of the surrounding soil. Peak pore pressures in a confined clay buffer of 0·5 m thickness are about five times than that in an unconfined (infinite) homogeneous clay medium. A substantial dependence of displacements of an inner clay core on the permeability of the surrounding medium is noted. Present mathematical modelling confirms the significance of thermodynamically coupled flow on near-field response as reported in the literature and provides a theoretical framework for modelling purposes. In practical applications of the present model, the importance of experimental determination of relevant material parameters should be highlighted.

ACKNOWLEDGEMENTS

The work presented in this paper was supported by the Natural Sciences and Engineering Research Council of Canada and Atomic Energy Canada Ltd.

REFERENCES

1. D. J. Cameron, 'Fuel isolation research for the Canadian nuclear fuel waste management program', Atomic Energy of Canada Ltd. *Report AECL-6834*, 1982.
2. G. L. McVay (ed.), *Scientific Basis for Nuclear Waste Management VII*, *Vol.* 26, Elsevier Science, North-Holland, New York, 1984.
3. J. P. Oliver, 'Radioactive waste management in OECD countries national programs and joint activities', *Proc. 2nd Int. Conf. Radioactive Waste Management*, Winnipeg, Canada, 1986.
4. S. T. Horseman and T. J. McEwen, 'Thermal constraints on disposal of heat-emitting waste in argillaceous rocks', *Engng. Geol*., **41,** 5–16 (1996).
5. R. L. Schiffman, 'A thermoelastic theory of consolidation', *Environmental and Geophysical Heat Transfer*, ASME, New York, 1971, pp. 78–84.
6. W. Derski and S. J. Kowalski, 'Equations of linear thermoconsolidation', *Arch. Mech*., **31,** 303–316 (1979).
7. J. R. Booker and C. Savvidou, 'Consolidation around a point heat source', *Int. J. Numer. Anal. Meth. Geomech*., **9,** 173–184 (1985).
8. D. McTigue, 'Thermoelastic response of fluid-saturated porous rock', *J. Geophys. Res*., **91,** 9533–9542 (1986).
9. M. Kurashige, 'A thermoelastic theory of fluid-filled porous materials', *Int. J. Solids Struct*., **25,** 1039–1052 (1989).
10. D. McTigue, 'Flow to a heated borehole in porous, thermoelastic rock: Analysis', *Water Resour. Res*., **26,** 1763–1774 (1990).
11. D. Smith, D. and J. R. Booker, 'Green's functions for a fully coupled thermoporoelastic material', *Int. J. Numer. Anal. Meth. Geomech*., **17,** 139–163 (1993).
12. H. N. Seneviratne, J. P. Carter and J. R. Booker, 'Analysis of fully coupled thermomechanical behaviour around a rigid cylindrical heat source buried in clay', *Int. Numer. Anal. Meth. Geomech*., **18,** 177–203 (1994).
13. Q. Jiang and R. K. N. D. Rajapakse, 'On coupoled heat-moisture transfer in deformable porous media', *Quart. J. Mech. Appl. Math*., **47,** 53–68 (1994).
14. Y. Wang and E. Papamichos, 'Conductive heat flow and thermal induced fluid flow around a well bore in a poroelastic medium', *Water Resour. Res*., **30,** 3375–3384 (1994).
15. G. Rehbinder, 'Analytical solutions of stationary coupled thermo-hydro-mechancial problems', *Int. J. Rock Mech. Min. Sci. Geomech. Abstr*., **32,** 453–463 (1995).
16. M. A. Biot, 'General solutions of the equations of elasticity and consolidation for a porous material', *J. Appl. Mech*., **23,** 91–96, (1956).
17. D. D. Fitts, *Nonequilibrium Thermodynamics: a Phenomenological Theory of Irreversible Processes in Fluid Systems*, McGraw-Hill, New York, 1962.
18. L. Onsager, 'Reciprocal relations in irreversible processes. I.', *Phys. Rev*., **37,** 403–426 (1931).
19. R. C. Srivastava and P. K. Avasthi, 'Non-equilibrium thermodynamics of thermo-osmosis of water through kaolinite', *J. Hydrol*., **24,** 111–120 (1975).
20. C. L. Carnahan, 'Thermodynamic coupling of heat and matter flows in near-field regions of nuclear waste repositories', *Proc. Mat. Res. Soc. Symp*., *Vol.* 26, 1984, pp. 1023–1030.
21. J. Letey and W. D. Kemper, 'Movement of water and salt through a clay-water system: experimental verification of Onsager's reciprocal relation', *Soil Sci. Soc. Am. Proc*., **33,** 25–29 (1969).
22. Y. Zhou, R. K. N. D. Rajapakse and J. Graham, 'A coupled thermoporoelastic model with thermo-osmosis and thermal-filtration', Special Issue on Poroelasticity *Int. J. Solids Struct*., 1998, (accepted.)
23. J. Bear and Y. Bachmat, *Introduction to Modeling of Transport Phenomena in Porous Media*, Kluwer Academic Publishers, London, 1990.
24. B. Davies and B. Martin, 'Numerical inversion of Laplace transform: a survey and comparison of methods', *J. Comput. Phys*., **33,** 1–32 (1979).
25. H. Stehfest, 'Numerical inversion of Laplace transforms', *Commun. Ass. Comput. Mach*., **13,** 47–49 (1970).
26. R. K. N. D. Rajapakse, 'Stress analysis of borehole in poroelastic medium', *J. Engng Mech*., **119,** 1205–1227 (1993).
27. M. Abramowitz and A. Stegum, '*Handbook of Mathematical Functions*, Dover, New York, 1965.
28. N. Tanaka and J. Graham, 'Pore water pressures in undrained triaxial tests with heating', *Proc. 2nd Int. Cong. Environmental Geotechnics*, Osaka, Japan, 1996.

